JOURNAL OF Materials CHEMISTRY

Structural, electrical and magnetic properties of low-dimensional conductors based on unsymmetrical π donor EDT-TTF and analogous selenium-substituted molecules

Akane Sato,[a] Emiko Ojima,[a] Hayao Kobayashi*[a] and Akiko Kobayashi[b]

[a]*Institute for Molecular Science, Okazaki 444-8585, Japan*
[b]*Department of Chemistry, School of Science, The University of Tokyo, Hongo, Bunkyo-ku 113-0033, Japan*

Received 24th March 1999, Accepted 24th June 1999

Organic conductors based on the unsymmetrical π donor molecule EDT-TTF (ethylenedithiotetrathiafulvalene) or its selenium-substituted analogs (EDST, EDTS) and tetrahedral anions $GaCl_4^-$ were prepared. The crystal structure determinations and the extended Hückel tight-binding band calculations indicate these systems to be quasi-one-dimensional conductors similar to TMTTF or TMTSF systems (TM systems). Electrical resistivity and magnetic susceptibility measurements and low-temperature X-ray diffraction experiments suggested a spin-Peierls ground state for $(EDT\text{-}TTF)_2GaCl_4$. $(EDST)_2GaCl_4$ and $(EDTS)_2GaCl_4$ exhibit metallic behavior down to *ca.* 40 K. The electric and magnetic properties of $(EDST)_2GaCl_4$ suggested a semimetallic state at low temperature. In spite of the similarity in the crystal and electronic band structures between TM and EDT systems, these two series of quasi-one-dimensional conductors do not share the same 'generalized phase diagram'. The electron–lattice interaction seems to be important in EDT conductors. The electric and magnetic properties of the isostructural systems with magnetic $FeCl_4^-$ anions were also examined. The magnetic interaction between the high-spin Fe^{3+} ions was found to be very weak.

Introduction

Since the discovery of the first organic superconductor $(TMTSF)_2PF_6$ (TMTSF = tetramethyltetraselenafulvalene) in 1980, the phase diagram of the $(TMTSF)_2X$ family ($X = PF_6^-$, AsF_6^-, ClO_4^-, …) has been studied intensively.[1] It is well known that the salts with octahedral anions such as PF_6^- and AsF_6^- undergo spin density wave (SDW) transitions around 12 K at ambient pressure. While $(TMTSF)_2ClO_4$ with tetrahedral anions has a ground state dependent on the cooling process: a superconducting state for a slow cooling process and an SDW state for a rapid cooling process. The physical properties of the sulfur-analogs $(TMTTF)_2X$ (TMTTF = tetramethyltetrathiafulvalene) have been also studied. In contrast to $(TMTSF)_2PF_6$, $(TMTTF)_2PF_6$ is a semiconductor below *ca.* 250 K and shows a spin-Peierls transition at about 20 K.[2–4] $(TMTSF)_2X$ and $(TMTTF)_2X$ are frequently referred to collectively as a TM_2X system (or more simply a TM system). The physical properties of the TM_2X system are changed systematically by changing the anion (X). The 'generalized pressure–temperature phase diagram' of the TM_2X system has been proposed by Jérome.[2] According to this famous diagram, $(TMTTF)_2PF_6$ takes a spin-Peierls state at 0–8 kbar and an SDW state at 8–37 kbar.[3] It is expected that the superconducting phase will be observed in the pressure range of 37–50 kbar. The electronic properties of $(TMTTF)_2PF_6$ can be converted into those of $(TMTSF)_2PF_6$ by applying *ca.* 30 kbar. That is, the exchange of S atoms to Se atoms is considered to produce the 'effective pressure (chemical pressure)'.

EDT-TTF (= ethylenedithiotetrathiafulvalene) is an unsymmetrical π donor molecule having the hybrid structure of TTF and BEDT-TTF (= bis(ethylenedithio)tetrathiafulvalene). EDT-TTF conductors with inorganic anions [*i.e.* AuI_2^-, $Au(CN)_2^-$, TaF_6^-, AsF_6^-, PF_6^-, ReO_4^-, ClO_4^-, BF_4^-][5–8] or transition metal complexes [$Ni(dmit)_2^-$, $Pd(dmit)_2^-$ and $Ni(dmise)_2^-$][9–12] have been reported. Except for the first ambient-pressure superconductor based on transition metal complexes, α-[EDT-TTF][$Ni(dmit)_2$][13] and its Pd-analogs, α′- and γ-[EDT-TTF][$Pd(dmit)_2$] with metallic (or semimetallic) ground states,[11,14,15] these EDT-TTF compounds with linear, octahedral and tetrahedral anions are highly conducting at room temperature but insulating at low temperature. Since the EDT-TTF conductors with inorganic anions have diadic columns and one-dimensional electronic structures similar to those of TM_2X, the effect of the selenium substitution on the electronic properties will be interesting. It is well known that typical organic superconductors such as TM_2X and κ-BEDT-TTF systems[16] have antiferromagnetic (or SDW) phases neighbouring superconducting phases. In these systems, spin excitation will be essential for realizing the superconducting states. Therefore it is desirable to know which of the electron correlation and the electron–lattice interaction is more important in the EDT-TTF and its selenium-substituted systems in order to see the possibility of a superconducting phase in these salts.

In this study, two selenium-substituted analogs of EDT-TTF, ethylenedithiodiselenadithiafulvalene (EDT-DSDTTF), which are named as 'EDTS' or 'EDST' depending on the selenium positions, were prepared and the conductors based on EDT-TTF, EDTS and EDST with tetrahedral $GaCl_4^-$ anions were synthesized. The analogous systems with the magnetic anion $FeCl_4^-$ were also prepared to examine the possibility of the interaction between π conduction electrons and localized magnetic moments in the anion sites (hereafter the conductors based on EDT-TTF, EDST and EDTS are called 'EDT systems'). Crystal structures, electrical conductivities and magnetic susceptibilities of $(EDT\text{-}TTF)_2GaCl_4$ (**1**), $(EDT\text{-}TTF)_2FeCl_4$ (**2**), $(EDST)_2GaCl_4$ (**3**), $(EDST)_2FeCl_4$ (**4**), $(EDTS)_2GaCl_4$ (**5**) and $(EDTS)_2FeCl_4$ (**6**) were examined. The crystal structures of **3** and **5** were also determined by X-ray diffraction at low temperature; in addition, low temperature X-ray oscillation photographs obtained for **1**, **2**, **3** and **5**, were analyzed. It should be mentioned here that the metallic compound of EDTS with linear anion IBr_2^- has already been reported by Papavassiliou *et al.* more than ten years ago.[17,18]

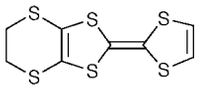

EDT-TTF

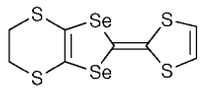

EDST

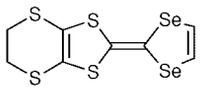

EDTS

Experimental

Synthesis of donors

EDT-TTF was synthesized following the previously reported procedure.[5] But we could not find a paper describing a synthetic procedure for EDST and EDTS.

EDST. A mixture of 4,5-ethylenedithio-1,3-diselenol-2-one[19] (1.0 g, 7.8 mmol) and 1,3-dithiole-2-thione (0.50 g, 1.7 mmol; Tokyo Kasei Industry) was stirred at 115 °C for 1 hour in $P(OEt)_3$ (20 ml) under a nitrogen atmosphere until the color of the solution turned from yellow to red. This red solution was cooled down to 40 °C and concentrated. A mixture of this concentrated solution and 10 ml of *n*-hexane was cooled and kept at −30 °C for 2 hours. The produced brown–orange solid was filtrated off, dried *in vacuo* and then dissolved in chloroform. After filtering out the brown powder of a minor product, BETS (=bis(ethylenedithio)tetraselenafulvalene), the orange solution was evaporated. The reddish–orange needles (132 mg) were obtained by fractional recrystallization in a yield of 20%.

EDTS. A mixture of 4,5-ethylenedithio-1,3-dithiole-2-thione (1.4 g, 6.1 mg)[20] and 4,5-bis(methoxycarbonyl)-1,3-diselenol-2-one[21] (0.1 g, 3.0 mmol) was stirred at 110 °C in 35 ml of toluene under a nitrogen atmosphere. Triethyl phosphite (35 ml) was added to the reaction solution, then the color of the solution turned immediately from yellow to red. This solution was refluxed at 110–120 °C for 2 hours until the color of solution changed from red to dark orange. This dark orange solution was evaporated and dried *in vacuo*. The red–purple oily residue was purified by silica gel column chromatography using carbon disulfide as eluent. The purple fraction was evaporated and the dark red oil of the intermediate (513 mg) was obtained in a yield of 33%. A red solution of the above-mentioned intermediate (513 mg, 1.0 mmol) and $LiBr{\cdot}H_2O$ (1.06 g, 10.2 mmol) dissolved in 70 ml of hexamethylphosphoric triamide (HMPA) was evacuated at room temperature for 2 hours in order to remove the amine impurity contained in HMPA from the solvent. After being bubbled by argon gas for 15 minutes, this solution was heated up to 90 °C for 1 hour and at 110 °C for 1 hour. The reaction mixture was extracted three times with benzene and washed five times with distilled water. The extract was dried over Na_2SO_4 for 50 minutes and the orange portion was evaporated. The orange residue was purified by silica gel column chromatography using carbon disulfide and dichloromethane as eluent. The orange solution was evaporated and dried *in vacuo*. The resulting orange powder was recrystallized from CS_2 to afford reddish–orange needle crystals (166 mg) in a yield of 43%.

Crystal preparation

Single crystals of **1**–**6** were obtained by electrochemical oxidation in a two compartment glass H-cell equipped with platinum wires as the electrodes. The solutions of dichloromethane (20 cm^3) containing the donor (EDT-TTF, EDST or EDTS; 10 mg) and $[(C_2H_5)_4N]MCl_4$ ($M=Ga^{3+}$ or Fe^{3+}; 100 mg) were applied by a constant current of 0.9 μA at 20 °C under a nitrogen atmosphere.

X-Ray experiments

Crystal structures of **1**–**6** were determined at room temperature and those of **3** and **5** were also determined at low temperature. Crystallographic data are summarized in Table 1. Intensity data of the room-temperature structures were collected by an automatic four-circle diffractometer (Rigaku AFC-5R or Rigaku AFC-7R) equipped with a rotating anode (Mo-Kα). The $\omega-2\theta$ scan was adopted. Lattice parameters were determined by using 20–27 reflections. Semiempirical absorption corrections were made. For low-temperature experiments, a Weissenberg-type imaging plate system [DIP320 (MAC Science Company)] equipped with a Mo-Kα rotating anode and a helium cryostat was used.

The crystal structures were solved by direct methods and refined by full matrix least-squares methods. Full crystallographic details, excluding structure factors, have been deposited at the Cambridge Crystallographic Data Centre (CCDC).† Oscillation photographs of **1**, **2**, **3** and **5** were taken down to 7 K.

Electrical resistivity and magnetic susceptibility measurements

Temperature dependencies of the electrical resistivities were measured along the stacking direction of donor molecules ($\|c$ axis) in the temperature range of 4–300 K at ambient pressure. The high-pressure resistivities of **3** were measured up to 16 kbar by using a clamp-type high-pressure cell. The magnetic susceptibilities of polycrystalline samples were measured by a SQUID magnetometer (MPMS2, MPMS7) down to 2 K. Applied magnetic fields were: 5 and 70 kOe for **1**, **3** and **5**; 5 and 10 kOe for **2**, **4** and **6**. The anisotropy of the susceptibilities of **5** was measured on a single crystal of about 3 mg, where the magnetic field (10 kOe) was applied approximately parallel to the *a*, *b* and *c* axes. Paramagnetic susceptibilities were obtained by subtracting Pascal's diamagnetic contributions.

Results and discussion

Crystal and electronic structures

All the compounds (**1**–**6**) are isostructural with each other but not isostructural with the previously reported EDT-TTF conductors with tetrahedral anions such as ClO_4^-, BF_4^- and ReO_4^- with monoclinic *C*2/*c* symmetry.[5] Crystals belong to the monoclinic system with space group $P2_1/m$. As shown in Fig. 1(a), the unit cell contains four donors on the general positions and two anions on the mirror planes. Unlike the orientation of the tetrahedral anion (X) in the TM_2X system ($X=ClO_4^-$, BF_4^-,...) located on the inversion center, the orientation of MCl_4 (M=Ga, Fe) is not disordered. The donor molecules were almost flat except for the ethylene group with eclipsed conformations. Similar to $(EDT\text{-}TTF)_2X$ ($X=AuI_2^-$, $Au(CN)_2^-$, TaF_6^-, AsF_6^-, PF_6^-, ReO_4^-, ClO_4^- and BF_4^-),[5] donor molecules were stacked to form diadic columns, where donor molecules overlap each other in a head-to-tail manner [Fig. 1(b)].

The extended Hückel tight-binding bands were calculated. Intermolecular overlap integrals of HOMOs (highest occupied molecular orbitals) of **1**, **3** and **5** are given in Table 2, from which the conduction bands are formed. Similar to the case of the TM system, two overlap integrals along the stacking axis of donors [*a* and *b* (see Table 2)] are approximately equal to each other. As was expected, they are enhanced by the selenium-

†CCDC reference number 1145/168. See http://www.rsc.org/suppdata/jm/1999/2365 for crystallographic files in .cif format.

Table 1 Summary of measurements and crystal data for **1–6**

	1	**2**	**3**		**4**	**5**		**6**
Chemical formula	$C_{16}Cl_4H_{12}GaS_{12}$	$C_{16}Cl_4H_{12}FeS_{12}$	$C_{16}Cl_4H_{12}GaS_8Se_4$		$C_{16}Cl_4H_{12}GaS_8Se_4$	$C_{16}Cl_4H_{12}GaS_8Se_4$		$C_{16}Cl_4H_{12}FeS_8Se_4$
Temperature/K	293	293	293	17	293	293	7	293
Formula weight	800.52	786.65	988.12	988.12	974.25	988.12	988.12	974.25
Crystal system	Monoclinic	Monoclinic	Monoclinic	Monoclinic	Monoclinic	Monoclinic	Monoclinic	Monoclinic
Space group	$P2_1/m$	$P2_1/m$	$P2_1/m$	$P2_1/m$	$P2_1/m$	$P2_1/m$	$P2_1/m$	$P2_1/m$
a/Å	6.586(4)	6.587(3)	6.647(2)	6.6090	6.645(5)	6.543(6)	6.632	6.646(4)
b/Å	30.438(4)	30.419(4)	30.714(4)	30.4510	30.701(4)	30.395(7)	30.402	30.352(4)
c/Å	7.091(4)	7.081(4)	7.138(5)	6.9270	7.136(5)	7.251(7)	7.0891	7.247(3)
β/degrees	100.09(5)	100.04(4)	100.14(4)	100.257	100.03(6)	100.37(8)	100.472	100.36(4)
V/Å^3	1399(1)	1397(1)	1434(1)	1385.99	1433(1)	1440(2)	1405.5	1438.0(9)
Z	2	2	2	2	2	2	2	2
μ (Mo-Kα)/cm^{-1}	22.69	69.99	69.99	72.45	65.69	69.1	69.1	65.5
Total reflections	3563	4477	3642	10923	4590	4624	12473	4612
Unique reflections	3297	4167	3371	4295	4274	4305	4394	4295
R_{int}	0.053	0.035	0.055	0.048	0.032	0.041	0.058	0.034
R, R_w	0.058, 0.046	0.044, 0.035	0.029, 0.021	0.083, 0.110	0.042, 0.044	0.039, 0.065	0.091, 0.111	0.038, 0.047

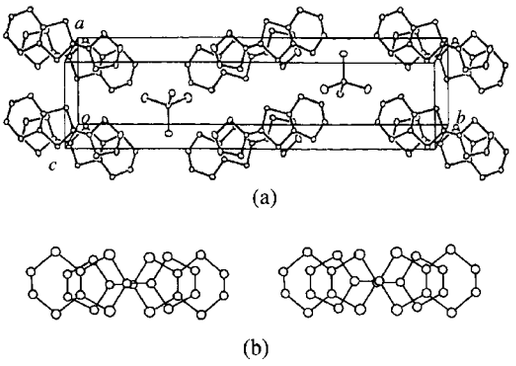

Fig. 1 (a) Crystal structure and (b) two independent overlapping modes of donor molecules in (EDT-TTF)$_2$GaCl$_4$ (**1**).

Table 2 The overlap integrals of **1**, **3** and **5**

	1	**3**	**5**
a	29.3	61.3	40.8
b	25.2	59.8	44.7
a*/*b	1.16	1.02	1.09 (=*b*/*a*)
***p*1=*p*2**	0.04	4.8	3.06
q	6.13	24.4	19.4
r	5.3	11.8	8.83

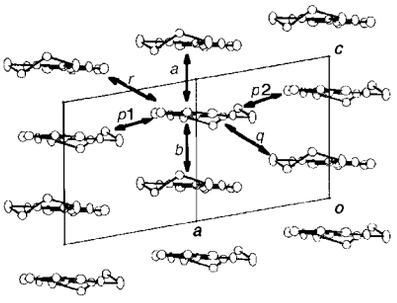

substitution. The ratio of a (or b) to q (the largest transverse interaction) of **1** is much larger than those of **3** and **5**: a (or b): q 4.5 (**1**), 2.5 (**3**), 2.2 (**5**). This means that the two-dimensionality is enhanced by the introduction of selenium atoms. The energy dispersion curves and quasi-one-dimensional Fermi surfaces are shown in Fig. 2.

Electrical resistivities

Temperature dependencies of the electrical resistivities of **1**–**5** are shown in Fig. 3. The crystals of **1** and **2** are semiconducting. The room-temperature resistivities of these salts (ρ_{RT}) were 0.2–0.1 Ω cm. The log ρ *vs.* T^{-1} plot of **1** gave the activation energies (Δ) of 17 and 12 meV at the temperature ranges of 100–200 K and 40–100 K, respectively. The high-pressure resistivity measurement of **1** showed that the system remains semiconducting at least up to 5 kbar. Since only the room-temperature conductivities and the metal–insulator transition temperatures (T_{MI}) were presented in the previous paper,[5] the temperature dependencies of resistivities of (EDT-TTF)$_2$BF$_4$ and (EDT-TTF)$_2$TaF$_6$ obtained previously are given in Fig. 4 and 5 for comparison. Unlike GaCl$_4$ (**1**) and FeCl$_4$ (**2**) salts, BF$_4$ and TaF$_6$ salts show clear transitions from the weakly metallic states to the insulating states around 110 and 50 K, respectively.[5]‡ The resistivity behavior of (EDT-TTF)$_2$TaF$_6$

‡In the previous report (ref. 5), the M–I transition temperature of (EDT-TTF)$_2$BF$_4$ was erroneously reported to be 170 K.

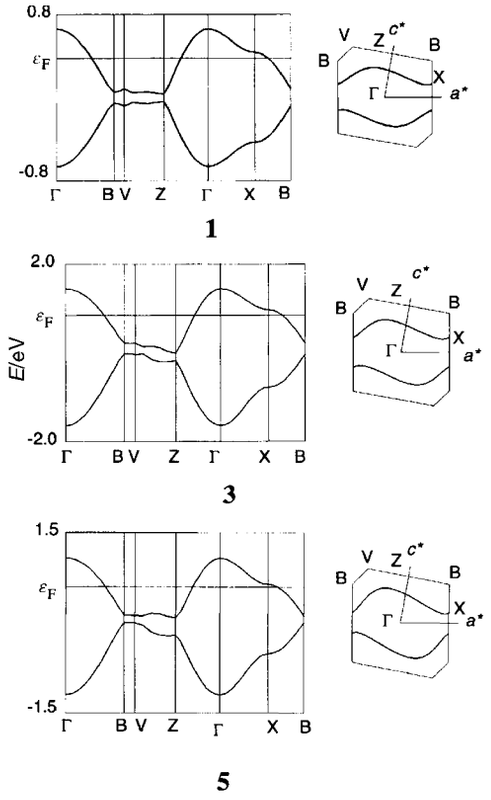

Fig. 2 Extended-Hückel tight-binding bands and Fermi surfaces of $(EDT\text{-}TTF)_2GaCl_4$ (**1**), $(EDST)_2GaCl_4$ (**3**) and $(EDTS)_2GaCl_4$ (**5**).

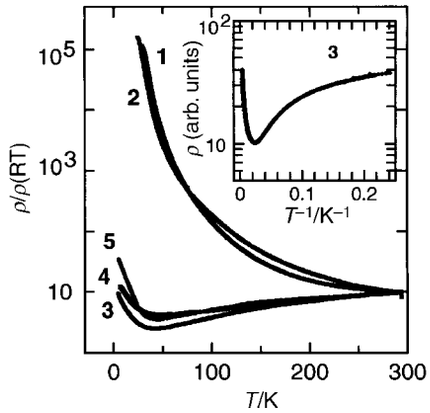

Fig. 3 Temperature dependencies of the electrical resistivities of **1**–**5**. The resistivities were measured along the *c* axes. The log ρ *vs.* T^{-1} plot of **3** is shown in the inset.

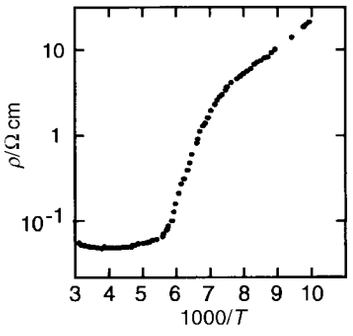

Fig. 4 Temperature dependence of electrical resistivity of $(EDT\text{-}TTF)_2BF_4$. The measurements were made along the *b* direction (stacking direction of EDT-TTF).

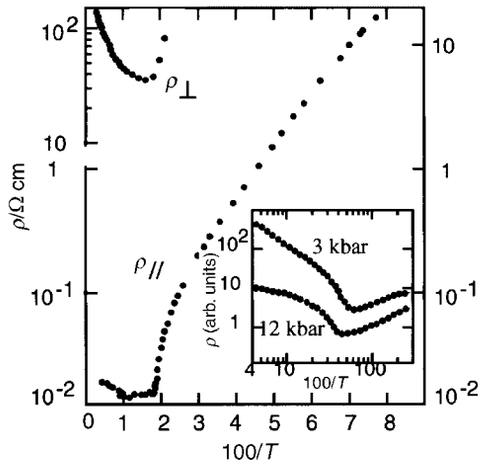

Fig. 5 Temperature dependence of the electrical resistivity of $(EDT\text{-}TTF)_2TaF_6$. $\rho_{\|}$ and $\rho_\perp$ are the resistivities along and perpendicular to the *bc* plane (conduction plane), respectively.

resembles that of $(EDST)_2GaCl_4$ (**3**) or $(EDTS)_2GaCl_4$ (**5**) rather than that of $(EDT\text{-}TTF)_2GaCl_4$ (**1**) constructed from the same donor molecules. This will be related to the difference in the crystal structures.

Since the band width is enhanced by introducing the selenium atoms, metallic nature will be expected in the EDST and EDTS systems. In fact, unlike EDT-TTF salts (**1**, **2**), **3**–**6** were metallic down to about 40 K ($\rho_{RT}/\rho_{40\ K} \approx 3.5$) below which very sluggish and sample-dependent resistivity increases were observed. The room-temperature resistivities were 0.2–0.03 Ω cm. The typical example of the log ρ *vs.* T^{-1} plot of **3** is shown in the inset of Fig. 3. The resistivity tended to be saturated below 10 K and the system retained high conductivity even at 4 K. This indicates the semimetallic nature of the ground state. High-pressure resistivity measurements were carried out on **3** (Fig. 6). The metallic nature was enhanced with increasing pressure but the resistivity increase at low temperature could not be suppressed completely up to 16 kbar. Similar pressure dependence of the resistivity was also observed in $(EDT\text{-}TTF)_2TaF_6$ (see the inset of Fig. 5).

Magnetic susceptibilities

Temperature dependencies of the magnetic susceptibilities of polycrystalline samples of **1**, **3** and **5** are shown in Fig. 7. Due to the small magnetization, the datum points were somewhat scattered. The paramagnetic susceptibility of **1** decreased gradually with lowering temperature at 70–300 K. The room-temperature susceptibility was about 1.6×10^{-4} emu mol^{-1} which is a little smaller than the Pauli paramagnetic susceptibility of typical organic metals. The semiconducting behavior

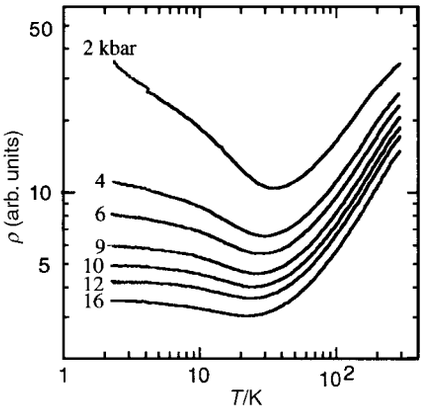

Fig. 6 Resistivities of $(EDST)_2GaCl_4$ (**3**) at high pressure.

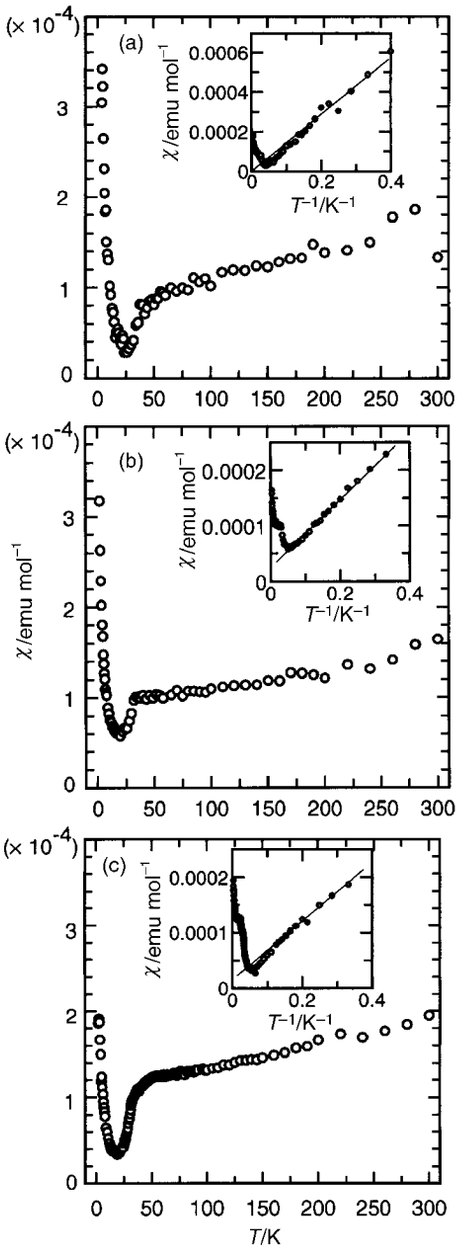

Fig. 7 Magnetic susceptibilities of (a) **1** (EDT-TTF)$_2$GaCl$_4$, (b) **3** (EDST)$_2$GaCl$_4$ and (c) **5** (EDTS)$_2$GaCl$_4$. The Pascal's diamagnetic corrections were made.

and the paramagnetic susceptibility show that the system is not in a simple band insulating state above 50 K. In order to subtract the contribution of paramagnetic impurities at low temperature, a χ *vs.* $1/T$ plot was made ($\chi = C/T + \chi_0$): **1**, $C = 1.5 \times 10^{-3}$ emu K mol^{-1}, $\chi_0 \approx 0$; **3**, $C = 5 \times 10^{-4}$ emu K mol^{-1}, $\chi_0 \approx 2.5 \times 10^{-5}$ emu mol^{-1}; **5**, $C = 5 \times 10^{-4}$ emu K mol^{-1}, $\chi_0 \approx 1.3 \times 10^{-5}$ emu mol^{-1} (see the inset of Fig. 7). Obtained Curie contributions (C) correspond to the contents of 0.16% (**1**), 0.03% (**3**) and 0.03% (**5**) of free $S = 1/2$ spins per formula unit. The χ_0-value of **1** was estimated to be zero and the susceptibility drop around 50 K was almost field-independent up to 70 kOe. These facts suggest that (EDT-TTF)$_2$GaCl$_4$ (**1**) undergoes a spin-Peierls transition around 50 K.

The magnetic susceptibilities of **3** and **5** decreased gradually down to 40 K and then decreased abruptly. Similar to the case of **1**, sharp decreases in the susceptibilities of **3** and **5** were also observed under a magnetic field of 70 kOe. However, in contrast to the zero χ_0-value of **1**, χ_0 of **3** and **5** were not zero. The small paramagnetic susceptibilities (2.5×10^{-5} (**3**) and 1.3×10^{-5} (**5**) emu mol^{-1}) are consistent with incomplete nesting of Fermi surfaces (that is, the semimetallic states) below 40 K, suggested by the resistivity measurements. The single crystal susceptibilities of **5** for the magnetic field parallel to the *a*-, *b*- and *c*-axes are given in Fig. 8. The susceptibilities were decreased almost isotropically below 40 K, which ruled out the possibilities of an SDW ground state.

Recently, there has been an increasing interest in systems where the interaction between π conduction electrons and localized magnetic moments of $FeCl_4^-$ anions produces novel π–d coupled electronic properties.[22] Therefore the salts **2**, **4** and **6** with $FeCl_4^-$ anions were examined in anticipation of a possible magnetic interaction between the localized spins of Fe^{3+} mediated by π electrons of donor molecules. However, the Fe^{3+} magnetic moments were found to be almost independent of each other in these systems. The temperature dependences of the susceptibilities of **2**, **4** and **6** satisfied the Curie law (Fig. 9). The large susceptibilities originate from the high-spin state of Fe^{3+} ions. By assuming $S = 5/2$ and $g = 2$ and neglecting the susceptibility of π conduction electrons, the spin concentrations of **2**, **4** and **6** were estimated to be 0.98 (**2**), 0.97 (**4**) and 0.99 (**6**). The Curie–Weiss plot suggested weak antiferromagnetic interactions ($\theta < 1.4$ K). No indication of the magnetic transition was observed down to 2 K.

Structure modification at low temperature

X-Ray oscillation photographs of **1** taken at 300 and 7 K are shown in Fig. 10. Below 50 K, new X-ray spots were observed between the layers of main Bragg reflections, indicating doubling of the lattice constant *c*. Thus, the magnetic transition around 50 K was confirmed to be a spin-Peierls transition, as suggested above. Similar extra spots were also observed in **2** at 7 K, indicating the non-magnetic state of the π electron system at low temperature.

X-Ray experiments were also carried out on **3** and **5**. However, no extra spots were observed below 40 K. Therefore the distortion of the crystal lattice will be small even if it

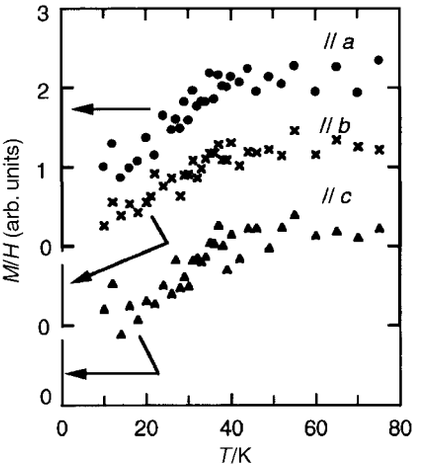

Fig. 8 The susceptibilities of (EDTS)$_2$GaCl$_4$ (**5**) for the magnetic field (10 kOe) parallel to *a*, *b* and *c* axes.

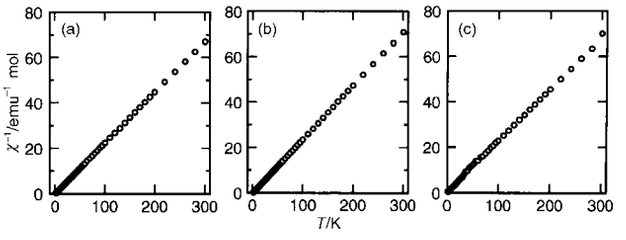

Fig. 9 The magnetic susceptibilities of (a) **2** (EDT-TTF)$_2$FeCl$_4$, (b) **4** (EDST)$_2$FeCl$_4$ and (c) **6** (EDTS)$_2$FeCl$_4$. The Pascal's diamagnetic contributions were subtracted.

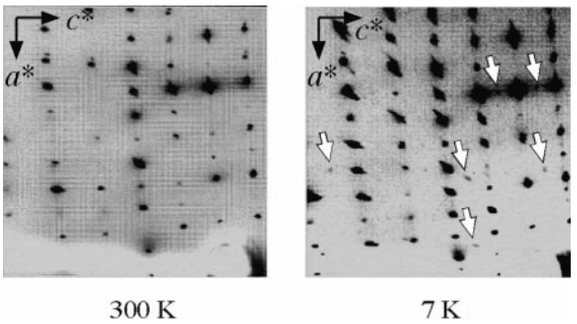

Fig. 10 X-Ray oscillation photographs of $(EDT\text{-}TTF)_2GaCl_4$ (**1**) at 300 and 7 K. The arrows indicate extra reflections observed below *ca.* 50 K.

develops below 40 K. This would be consistent with the incomplete nesting of the Fermi surfaces suggested from the electric and magnetic properties. Temperature dependences of the lattice constants of **3** were examined. But the lattice constants could not be determined accurately enough to detect the possible anomaly around 40 K. Roughly speaking, the lattice constants are linearly dependent on temperature. Thermal expansion coefficients (α) are: $\alpha_a = 9.59 \times 10^{-5}\ K^{-1}$, $\alpha_b = 1.73 \times 10^{-5}\ K^{-1}$, $\alpha_c = 2.71 \times 10^{-5}\ K^{-1}$, $\alpha_V = 1.46 \times 10^{-5}\ K^{-1}$. The low-temperature crystal structures of **3** and **5** were determined at 17 and 7 K, respectively. But no significant structural change was observed. The intermolecular distances of donor molecules are 3.46 (3.56) and 3.47 (3.60) Å for **3** at 17 K (the values in parentheses are the room-temperature ones) and 3.51 (3.56) and 3.69 (3.61) Å for **5** at 7 K.

We have previously carried out X-ray diffuse scattering experiments on $(EDT\text{-}TTF)_2TaF_6$.[6] As shown in Fig. 11, extra X-ray spots similar to those observed in **1** appeared below *ca.* 50 K (T_{MI}). Since $(EDT\text{-}TTF)_2TaF_6$ transforms from the weakly metallic state to the insulating state around 50 K (see Fig. 4), the result of this X-ray experiment shows that $(EDT\text{-}TTF)_2TaF_6$ has a Peierls insulating [or CDW (charge density wave)] ground state. The low-temperature resistivities of $(EDT\text{-}TTF)_2TaF_6$ gave an energy gap of about 1.6 meV, which is approximately equal to the energy gap expected from the mean-field theory of Peierls transition ($2\Delta/T_{MI} \approx 3.5$). The complete nesting of the Fermi surfaces (that is, the insulating ground state) is consistent with the relatively weak two-dimensionality in EDT-TTF systems. Anyway it becomes clear that the phase diagram of EDT systems contains a region of the CDW phase, which is not found in the generalized phase diagram of TM systems.

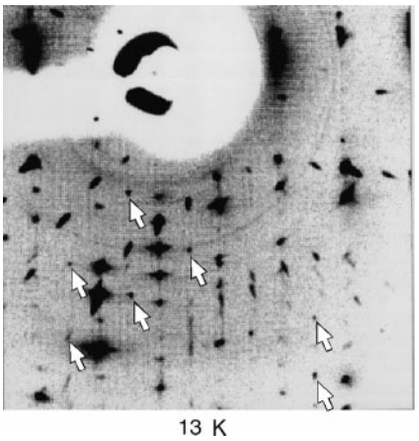

Fig. 11 X-Ray oscillation photographs of $(EDT\text{-}TTF)_2TaF_6$ at 13 K. The arrows indicate examples of extra reflections developed below 50 K.

On the ground states of EDT-systems

As mentioned before, the extended Hückel band structure calculations suggested the EDT-TTF salts (**1** and **2**) to be quasi 1D metals. However, the semiconducting behavior of these salts shows the calculated Fermi surfaces to be artificial. As is well known, this discrepancy is considered to originate from the effect of Coulomb repulsion (U), which makes the system an insulator when $U \gg t$ (transfer integral). Usually, the difference between the first and second oxidation potentials ($\Delta E = E^2_{1/2} - E^1_{1/2}$) of the donor molecule is used as a measure of U. The ΔE-values of EDT-TTF, EDST and EDTS were determined in this study from the cyclic voltammograms: EDT-TTF 0.42 eV, EDST 0.35 eV, EDTS 0.37 eV. The relatively large ΔE and small intermolecular overlap integrals of EDT-TTF salts (see Table 2) suggest a tendency towards localization of the π electrons in **1** and **2**. This picture is consistent with the spin-Peierls transition of **1**. Needless to say, the spin-Peierls behavior of the π electron system of **2** is hidden by the large magnetic susceptibility due to the high-spin state of Fe ions.

In the systems of **3**–**6**, the temperature dependence of the resistivities suggests the transition from metallic state to semimetallic state or insulating state with a negligibly small energy gap below 40 K. As mentioned before, the magnetic properties of **5** ruled out the possibility of an SDW ground state and suggested the semimetallic state at low temperature, which is consistent with the possible weak lattice modulation indicated by X-ray experiments. The Curie term of the susceptibility and the very sluggish resistivity change at low temperature will be related to some lattice defects.

Since $(EDT\text{-}TTF)_2GaCl_4$ has a spin-Peierls ground state similar to $(TMTTF)_2PF_6$, it might be imagined that a superconducting EDT conductor will be discovered, if the selenium-substituted analogs are developed. However, the present study shows that the EDT family has a phase diagram different from that of TM_2X system. The CDW condensation observed in $(EDT\text{-}TTF)_2TaF_6$ and semimetallic properties in **3**–**6** at low temperature suggest the electron-lattice interaction to be important in EDT conductors.

References

1 D. Jérome, A. Mazaud, M. Ribault and K. Bechgaard, *J. Phys. Lett. (Paris)*, 1980, **41**, L-95.
2 D. Jérome and H. Schulz, *Adv. Phys.*, 1982, **31(4)**, 299; D. Jérome, *Science*, 1990, **253**, 1509.
3 J. Moser, M. Gabay, P. A. Senzier, D. Jérome, K. Bechgaard and J. M. Fabre, *Eur. Phys. J.*, 1999, **B1**, 39.
4 D. Jérome , in *Organic Conductors, Fundamentals and Applications*, ed. J.-P. Farges, Marcel Dekker, Inc., New York, Basel, Hong Kong, 1994.
5 (*a*) R. Kato, H. Kobayashi and A. Kobayashi, *Chem. Lett.*, 1989, 781; (*b*) A. Kobayashi, R. Kato and H. Kobayashi, in *The Physics and Chemistry of Organic Superconductors*, ed. G. Saito and S. Kagoshima, *Springer Proc. Phys.*, 1990, 51, 302.
6 A. Kobayashi *et al.*, Proceedings of the Annual Meeting of the Chemical Society of Japan, Kyoto, March, 1995, Abstr., p. 433.
7 T. Mori and H. Inokuchi, *Solid State Commun.*, 1989, **70(8)**, 823.
8 A. Hountas, A. Terzis, G. C. Papavassiliou, B. Holti, M. Burkle, C. W. Meyer and J. Zambounis, *Acta Crystallogr, Sect. C*, 1990, **46**, 228.
9 R. Kato, H. Kobayashi, A. Kobayashi, T. Naito, M. Tamura, H. Tajima and H. Kuroda, *Chem. Lett.*, 1989, 1839.
10 B. Garreau, B. Pomarede, C. Faulmann, J.-M. Fabre, P. Cassoux and J.-P. Legros, *C. R. Acad. Sci. Paris*, 1991, **313(2)**, 509.
11 A. Kobayashi, A. Sato, K. Kawano, T. Naito, H. Kobayashi and T. Watanabe, *J. Mater. Chem.*, 1995, **5**, 1671.
12 (*a*) T. Naito, A. Sato, K. Kawano, A. Tateno, H. Kobayashi and A. Kobayashi, *J. Chem. Soc., Chem. Commun.*, 1995, 351; (*b*) A. Kobayashi, T. Naito, A. Sato and H. Kobayashi, *Synth. Met.*, 1997, **86**, 1841.
13 (*a*) H. Tajima, M. Inokuchi, A. Kobayashi, T. Ohta, R. Kato, H. Kobayashi and H. Kuroda, *Chem. Lett.*, 1993, 1235; (*b*) H. Tajima, M. Inokuchi, S. Ikeda, M. Arifuku, T. Naito, M. Tamura, T. Ohta, A. Kobayashi, R. Kato, H. Kobayashi and

H. Kuroda, *Synth. Met.*, 1995, **70**, 1035; (*c*) M. Inokuchi, H. Tajima, T. Ohta, H. Kuroda, A. Kobayashi, A. Sato, T. Naito and H. Kobayashi, *J. Phys. Soc. Jpn.*, 1996, **65(2)**, 538; (*d*) H. Tajima, A. Kobayashi, Y. Ootuka, A. Sato, T. Naito and H. Kobayashi, *Synth. Met.*, 1996, **79**, 141; (*e*) H. Tajima, M. Inokuchi, A. Kobayashi, A. Sato, T. Naio, H. Kobayashi and H. Kuroda, *Synth. Met.*, 1997, **85**, 1585.
14 L. Brossard, M. Ribault, B. Garreau, B. Pomarède and P. Cassoux, *Europhys. Lett.*, 1992, **19**, 223.
15 L. Brossard, M. Ribault, M. L. Doublet, E. Canadell, B. Garreau and J. P. Legros, *Synth. Met.*, 1993, **56**, 2833.
16 J. M. Williams, J. R. Ferraro, R. J. Thorn, K. D. Carlson, U. Geiser, H. H. Wang, A. M. Kini and M.-H. Whangbo, *Organic Superconductors (Including Fullerenes)*, Prentice Hall, New Jersey, 1992.
17 A. Terzis, A. Hountas, A. E. Underhill, A. Clark, B. Kaye, B. Hilti, C. Mayer, J. Pfeiffer, S. Y. Yiannopoulos, G. Mousdis and G. C. Papavassiliou, *Synth. Met.*, 1988, **27**, B97.
18 G. V. Papavassiliou, G. A. Mousdis, J. S. Zambounis, A. Terzis, A. Hountas, B. Hilti, C. W. Mayer and J. Pfeiffer, *Synth. Met.*, 1988, **27**, B379.
19 R. Kato, H. Kobayashi and A. Kobayashi, *Synth. Met.*, 1991, **41–43**, 2093.
20 K. S. Varma, A. Bury, N. J. Harris and A. E. Underhill, *Synthesis*, 1987, 837.
21 C. M. Bolinger and T. B. Rauchfuss, *Inorg. Chem.*, 1982, **21**, 3947.
22 H. Kobayashi, H. Tomita, T. Naito, A. Kobayashi, F. Sakai, T. Watanabe and P. Cassoux, *J. Am. Chem. Soc.*, 1996, **118**, 368; H. Kobayashi, A. Sato, E. Arai, H. Akutsu, A. Kobayashi and P. Cassoux, *J. Am. Chem. Soc.*, 1997, **119**, 12 392; H. Akutsu, K. Kato, E. Ojima, H. Kobayashi, H. Tanaka, A. Kobayashi and P. Cassoux, *Phys. Rev.*, 1998, **B58**, 9294.

Paper 9/02347J